In conclusion we want to point out that the calculations were carried out with a lattice 21 × 21. Control calculations with a lattice 41 × 41 showed that the relative deviation of the sought values in the entire range of the calculation lay within 3%.

NOTATION

R, φ, z, cylindrical coordinates; r, φ, θ, cylindrical polar coordinates; R_0, z_0, coordinates of the point 0; v, w, u, velocity components in the system of cylindrical polar coordinates; ψ, flow function; ω, vorticity; ξ, η, new variables; p, pressure; Re, Reynolds number; $\Delta\xi$, $\Delta\eta$, steps of the lattice; H, vector of discrepancies of the Navier–Stokes equations; ΔX, ΔY, vectors of corrections for the sought solution.

LITERATURE CITED

1. M. I. Zhukovskii and Yu. E. Karyakin, "Calculation of swirl flow of gas in an axiradial diffuser when there are reverse flows," Energomashinostroenie, No. 8, 7-10 (1978).
2. V. V. Tret'yakov and V. I. Yagodkin, "Numerical investigation of laminar curved flow in an annular channel," Inzh.-Fiz. Zh., 34, No. 2, 273-280 (1978).
3. R. A. Gentry, R. E. Martin, and B. J. Daly, "An Eulerian differencing method for unsteady compressible flow problems," J. of Comput. Phys., No. 1, 87-118 (1966).
4. P. Roach, Computing Hydrodynamics [Russian translation], Mir, Moscow (1980).
5. C. H. Reinsch, "Smoothing by spline functions," Numerische Mathematik, No. 3, 177-183 (1967).

FINITE-DIFFERENCE SOLUTION OF THE CONJUGATE HEAT TRANSFER, NATURAL CONVECTION, AND SOLIDIFICATION PROBLEM

F. V. Nedopekin and S. S. Petrenko

UDC 532.54:536.252

A mathematical model of the solidification of a binary melt under convection conditions with a two-phase zone taken into account is formulated on the basis of average transfer equations. Results of a numerical solution are presented.

The solidification of binary alloys is characterized by the presence of an intermediate domain which is a heterogeneous mixture of the liquid and solid phases and a so-called two-phase zone. As is known, the reason for the formation of such a zone [1] is the development of concentration and kinetic supercooling.

Two approaches exist for the compilation of the heat, mass, and momentum balance equations for the two-phase zone in a mathematical description of melt solidification. In one formal replacement of the heterogeneous by a homogeneous medium is assumed, where the thermophysical parameters of the latter are defined as average. Then the process is described by equations for a homogeneous medium. Here can also be referred the method of using effective physical, experimentally determined, parameters in these equations.

The second approach, which possesses great generality, is based on the mechanics of multiphase media [2] and assumes the examination of the two-phase zone in the approximation of average macrocontinuums [3]. The selection of the averaging method is also quite important here. Averaging over the volume of macropoints, executed according to known rules, is the most natural.

In this paper, both approaches are applied in formulating the problem. The average heat and mass transfer differential equations

$$\rho\left[\xi c_1+(1-\xi)c_2\right]\frac{\partial T}{\partial t}+c_2\rho(1-\xi)\vec{V}\nabla T=\nabla\left[\lambda_1\nabla\xi T+\lambda_2\nabla(1-\xi)T\right]+L\rho\frac{\partial\xi}{\partial t}, \tag{1}$$

$$(1-\xi)\frac{\partial C}{\partial t}=\nabla\left[D\nabla(1-\xi)C\right]+(1-k)C\frac{\partial\xi}{\partial t} \tag{2}$$

Donetsk State University.

Translated from Inzhenerno-Fizicheskii Zhurnal, Vol. 47, No. 2, pp. 286-293, August, 1984. Original article submitted April 19, 1983.

0022-0841/84/4702-0959$08.50

are formulated by using the generalized balance equation for macropoints [3].

The flow of the melt is examined without taking account of the influence of the phase shrinkage, hence, the problem is formulated under the condition of approximate equality of the solid and liquid phase densities.

Equation (2) is obtained under the assumption that diffusion is negligible in the solid phase, while the impurity is distributed uniformly in the liquid within the limits of the macropoints. This permits expressing the mean impurity concentration relative to the interphasial surface in the solid phase in terms of the true mean-volume value of the concentration in the melt by the relationship $C_1 = kC$.

Melt motion in the liquid core of the ingot and in the liquid–solid domain of the two-phase zone is described, because of its temperature inhomogeneity, by the transport equation of the average velocity vortex Ω and the Poisson equation for the stream function Ψ:

$$\frac{\partial \Omega}{\partial t} + \vec{V}\nabla\Omega = \nabla(\nu\nabla\Omega) + g\beta\frac{\partial T}{\partial X}(1-\xi), \tag{3}$$

$$\Delta\Psi = -\Omega, \tag{4}$$

where $\nu = \nu_0(1 - 5\xi)$ is the effective kinematic viscosity coefficient taking the Einstein correction into account [4] under the assumption of disperseness of the medium in the domain of the two-phase zone.

The stream function Ψ is associated with the true mean-volume velocity of the melt by relationships satisfying the continuity equation for an incompressible fluid:

$$(1-\xi)V_x = \frac{\partial\Psi}{\partial Y}, \quad (1-\xi)Y_y = -\frac{\partial\Psi}{\partial X}.$$

System (1)-(4) can be closed by the equation of the liquidus line on the Fe–C phase diagram in conformity with the quasiequilibrium theory of the two-phase zone of Borisov [1]:

$$T = -\alpha C + T_{\text{к}}. \tag{5}$$

It should be noted that the formulated system (1)-(5) permits investigation of the thermal convection in not only the liquid core of the ingot but also in the liquid–solid domain of the two-phase zone ($0 \leqslant \xi \leqslant \xi_d$). The approximate "freezing" condition [5] is not relied upon here.

In dimensionless form (1)-(5) are written as follows

$$(1-\xi)\frac{\partial S}{\partial \mathrm{Fo}} = \frac{1}{\mathrm{Lu}}\Delta(1-\xi)S + (1-\xi)S\frac{\partial\xi}{\partial \mathrm{Fo}}, \tag{6}$$

$$c_e\frac{\partial\theta}{\partial \mathrm{Fo}} = \nabla[(1+\lambda\xi)\nabla\theta] + [\lambda\nabla\xi - (1-\xi)\vec{v}]\nabla\theta + \lambda\Delta\xi, \tag{7}$$

$$\frac{\partial\omega}{\partial \mathrm{Fo}} = \mathrm{Pr}\nabla[(1+5\xi)\nabla\omega] - \vec{v}\nabla\omega + \mathrm{Gr}^*\mathrm{Pr}^2(1-\xi)\frac{\partial\theta}{\partial x}, \tag{8}$$

$$\Delta\psi = -\omega, \tag{9}$$

$$\theta = -\varphi S + \varphi_0, \tag{10}$$

where $c_e = 1 + c\xi - W(\partial\xi/\partial\theta)$ is the modified specific heat, and $c = c_1/c_2 - 1$; $\lambda = \lambda_1/\lambda_2 - 1$; $\varphi = \alpha C_0/T_0$; $\varphi_0 = T_k/T_0$.

By using (10) the diffusion equation (6) is converted in the transport equation for a fraction of the solid phase [6]

$$(1-k)\,\mathrm{Lu}\frac{\partial\xi}{\partial \mathrm{Fo}} = \Delta\xi + \frac{2}{\theta-\varphi_0}\nabla\theta\nabla\xi - \frac{\mathrm{Lu}\dfrac{\partial\theta}{\partial \mathrm{Fo}} - \Delta\theta}{\theta-\varphi_0}(1-\xi) \tag{11}$$

In contrast to the system used in [7] system of equations (7)-(9), (11) formulated takes account of the contribution of components containing $\nabla\xi$ and $\Delta\xi$ to the mass- and heat-transfer processes. The value of these latter quantities can be quite substantial in the initial solidification stage when the two-phase zone is narrow and the distribution of ξ most inhomogeneous.

Formulation of the mathematical model is completed by formulating the boundary conditions. Because of axial symmetry, half the domain is considered. It is assumed that the temperature is distributed homogeneously over the whole domain at the initial instant, there is no solid phase, and the melt is fixed:

$$\theta|_{Fo=0} = 1, \quad \xi|_{Fo=0} = \omega|_{Fo=0} = \psi|_{Fo=0} = 0. \tag{12}$$

On the axis of symmetry Oy

$$\psi|_{x=0} = \omega|_{x=0} = \frac{\partial \xi}{\partial x}\Big|_{x=0} = \frac{\partial \theta}{\partial x}\Big|_{x=0} = 0. \tag{13}$$

The upper boundary of the domain (the mirror image of the melt) Γ_1 is heated by the exothermal charge, whose thermal action can, according to [8], be described as follows:

$$\frac{\partial (1 + \lambda\xi)\,\theta}{\partial y}\Big|_{\Gamma_1} = \begin{cases} 0, & 0 \leqslant Fo \leqslant Fo_1, \\ 0{,}12Fo/(Fo_2 - Fo_1), & Fo_1 < Fo < Fo_2, \\ 0{,}12, & Fo \geqslant Fo_2, \end{cases} \tag{14}$$

where $Fo_2 = 2Fo_1 = 0.254$ (2400 sec).

Processing the experimental data existing in the literature permits obtaining an expression also for the density of the heat flux along the normal to the ingot surface in a firebrick-heated feeder head (Γ_2) and its body (Γ_3), respectively:

$$\frac{\partial (1 + \lambda\xi)\,\theta}{\partial n}\Big|_{\Gamma_2} = \frac{0.059}{Fo + 0.692} - 0.0084, \tag{15}$$

$$\frac{\partial (1 + \lambda\xi)\,\theta}{\partial n}\Big|_{\Gamma_3} = \frac{0{,}0181}{Fo + 0{,}0121} + 0{,}161 \tag{16}$$

The boundary condition for (11) is determined from the condition of no average impurity concentration flux through the ingot surface $-(\vec{n} \times \nabla(1 - \xi)S)\,|_{\Gamma_1+\Gamma_2+\Gamma_3} = 0$, or taking (10) into account

$$(\vec{n} \cdot \nabla)[(1 - \xi)(\varphi_0 - \theta)]|_{\Gamma_1+\Gamma_2+\Gamma_3} = 0. \tag{17}$$

On the liquidus boundary (Γ_4) the following condition is valid

$$\xi|_{\Gamma_4} = 0. \tag{18}$$

On the boundaries Γ_1, Γ_2, Γ_3 and the decanting boundary Γ_5

$$\psi|_{\Gamma_1+\Gamma_2+\Gamma_3+\Gamma_5} = 0. \tag{19}$$

We determine the boundary conditions for (8) for the finite-difference approximation.

The presence of nonlinear and nonstationary differential equations in the system (7)-(9), (11) determines mainly the general structure of the algorithm. At each instant, solution of the whole system is divided into two stages (blocks). In the first, the solution is executed for (7) and (11), which are included in the interaction process relative to θ and ξ. In the second stage, (8) and (9) are solved, where the fields θ and ξ found in the first stage are used. Furthermore, the system is solved in the same sequence in the next instants, etc. Within the limits of the block, the two-dimensional equations are decomposed into one-dimensional equations by the method of variable directions with subsequent approximation of the one-dimensional equations by the monotonic scheme of A. A. Samarskii.

In particular, for the heat-transport equation (7) in the Ox direction, we have

$$\left[\frac{\partial}{\partial x}\left(k\frac{\partial \theta}{\partial x}\right) + r_1\frac{\partial \theta}{\partial x} - q\theta\right]^{n+0.5} = -\left[\frac{\partial}{\partial y}\left(k\frac{\partial \theta}{\partial y}\right) + r_2\frac{\partial \theta}{\partial y} + q\theta\right]^{n}, \tag{20}$$

where $k = 1 + \lambda\xi$; $r_1 = \lambda(\partial\xi/\partial x) - (1 - \xi)v_x$; $r_2 = \lambda(\partial\xi/\partial y) - (1 - \xi)v_y$; $q = c_e/0.5\tau - \lambda\Delta\xi$.

Subsequent application of the integrointerpolation method in combination with the method of perturbed coefficients [9] assures the conservativity and monotonicity of the implicit difference scheme of second-order accuracy. The difference equations are reduced to canonical form.

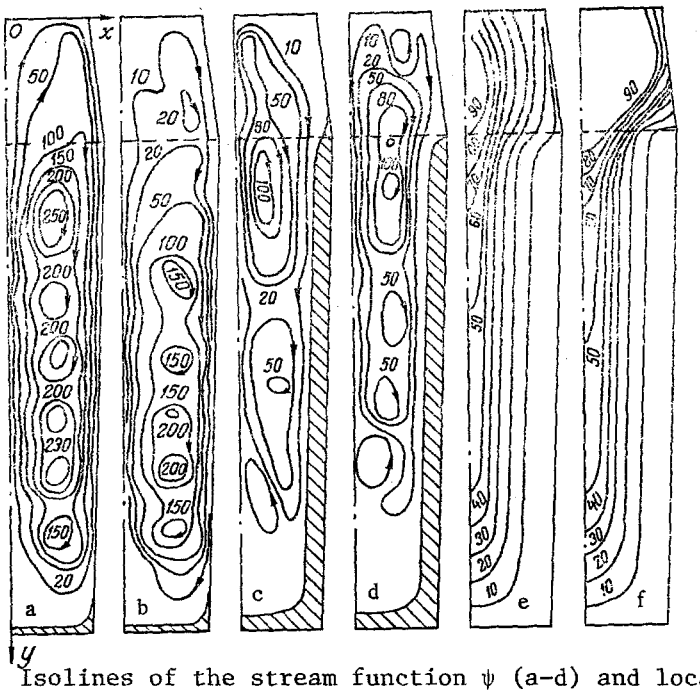

Fig. 1. Isolines of the stream function ψ (a-d) and location of the solidification boundaries (e, f) (numbers at the curves are time in min) for ingots heated by firebrick (a, c, d) and heat-insulated inserts (b, d, f), a, b) t = 1 min, c, d) t = 5 min.

For (20) we have

$$A_j\theta_{i,j-1}^{n+0.5} - C_j\theta_{i,j}^{n+0.5} + B_j\theta_{i,j+1}^{n+0.5} = -F_j^n, \tag{21}$$

where j = 1, 2, ..., N; i = 1, 2, ..., M is the number of mesh nodes along Ox and Oy, respectively, $\theta_{i,j}$ is the difference analog of $\theta(x, y, Fo)$, $A_j = k_j(\varkappa_j/\hbar_j - b_j^-)/h_j$; $B_j = k_{j+1}(\varkappa_j/\hbar_j + b^+j)/h_{j+1}$; $C_j = A_j + B_j + q_j$; $\varkappa_j = 1/(1 + R_j)$ is the "perturbation" coefficient, and $R_j = 0.5h_j|r_j|/k_j$; $b^{\pm}_j = 0.5(r_j \pm |r_j|)/k_j$.

Equations (8) and (11) are approximated in an analogous manner. The system of algebraic equations of the type (21) is solved by the factorization method.

The boundary conditions for (8) are obtained separately (in connection with the curvilinearity of the boundary) for the Ox and Oy directions by the expansion of ω into a Taylor series around points of the boundary on which the adhesion condition is satisfied:

$$\omega_{I,J} = -\left[\frac{2\psi_{I,J-1}}{h_J^2} + \left(\frac{\partial^2\psi}{\partial y^2}\right)_{I,J}\right], \quad \omega_{I,J} = -\left[\frac{2\psi_{I-1,J}}{h_I^2} + \left(\frac{\partial^2\psi}{\partial x^2}\right)_{I,J}\right]. \tag{22}$$

where I, J are the coordinates of the mesh boundary nodes. At the time when the whole metal is liquid, this boundary is the internal surface of the ingot mold, which is replaced by the decantability boundary as the melt solidifies. The number of nodes per nonsolidifying part of the melt is gradually reduced, consequently, the values of I and J for all the boundary points are determined in each time layer. In the case of agreement between the direction of the boundary surface and the direction of the coordinate planes during crystallization, condition (22) takes the form of the Thom condition [10]. The Poisson equation (9) is solved by the iteration method of varible directions.

A nonuniform 24 × 25 mesh with condensation at the solid boundaries and rarefaction around the Oy axis was used in the computation. Because of the slope of the side wall of the ingot mold, the lattice step h_N depends linearly on the number of lines i, which required appropriate correction of θ in the near-wall nodes. The time step τ varied between $0.3\cdot10^{-4}$-$0.3\cdot10^{-2}$ while the steps for the space coordinates were h_i = 0.02-0.33 and h_j = 0.02-0.05.

The computation was carried out for a three-ton sheet ingot of killed steel mark St. 3 under the following initial parameters C_0 = 0.16%, ΔT_0 = 4K, X_0 = 0.21 m, H/X_0 = 6.7, the coincity of the ingot is 1.75, c_1 = 696 J/kg•K, c_2 = 788 J/kg•K, $\lambda_1 \simeq \lambda_2$ = 26.5 W/m•K, $\alpha = 4.67\cdot10^{-6}$ m²/sec, $\nu_0 = 0.75\cdot10^{-6}$ m²/sec, $L = 2.74\cdot10^5$ J/kg, ξ_d = 0.2, $q_0 = 1.93\cdot10^5$ W/m².

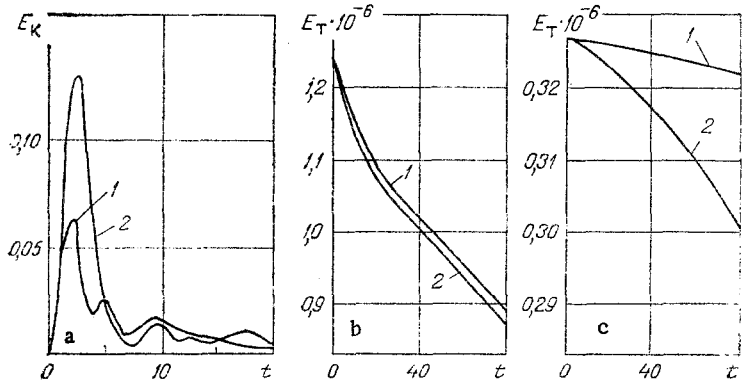

Fig. 2. Dependence on the time t (min): a) kinetic energy of the melt E_k (J), thermal energy E_T (J), b) ingot body, c) head part of the ingot; 1) heating by heat-insulated inserts; 2) by chamotte.

Analysis of the streamline behavior (Fig. 1) permits classification of the melt motion in the liquid core of the ingot as the flow in a vertical layer whose feature is the nuclear structure. Such a flow was observed in the solidification of a one-component melt with a plane interphasal boundary [11], as well as in experimental [12] and numerical [13] investigations of the natural convection in a vertical layer. The origination of secondary vortices is evidently associated with the hydrodynamic instability of the up and down flow [14]. The nuclear structure magnifies the heat transfer in the transverse direction of the domain. Considering the values of ψ within the limits of each vortex, it is easy to note that the most intensive melt motion occurs in the central part of the ingot in the initial solidification stage (Fig. 1a). The vortices with maximal intensity are localized with time in the upper half of the ingot (Fig. 1c). The values of ψ hence fluctuate with time. For a selected initial heating, the convection in the ingots lasts 30-35 min, the magnitude of the velocity during the first 14-16 min is reduced from ~3 to ~0.1 cm/sec.

The melt kinetic energy is pulsating in nature (Fig. 2a). A sudden flareup in convection intensity is observed within the first three minutes of solidification and caused the development of the maximal temperature gradient in this same period. Meanwhile, the thermal energy varies monotonely (Fig. 2b), which indicates its more conservative nature as compared with the kinetic energy.

In investigating the heat transfer between the ingot head and body, it is clarified that the heat does not yield heat to the ingot body during the first 2-3 min of solidification, but conversely, is its consumer (Fig. 3a). Later, the direction of the total heat flux Q becomes opposite on the ingot head-body boundary (Fig. 3b).

In the last stages of solidification Q grows. This is due to the rise in the gradient of T on the ingot head-body boundary because of liberation of the latent heat of crystallization of the still solidifying melt in the head together with the absence of this liberation in the almost solidified body of the ingot.

The convective motion of the melt in the liquid core and the two-phase zone affects the kinetics of solidification by increasing the rate of ingot solidifying. Moreover, growth of the two-phase zone is observed in the bottom part of the ingot in a vertical direction in addition to a diminution in its extent in the horizontal direction in a part under the head. Therefore, because of the development of the two-phase zone in the bottom part, conditions are degraded for "feeding" the solidifying ingot. As is known [15], this can contribute to the development of a physical inhomogeneity (the appearance of "bridges," secondary shrinkage blisters).

One of the most widespread methods of raising the yield of a workable metal is improvement of the heat insulating properties of the ingot mold heater. Hence, from the practical viewpoint it is important to know how the heat transport, hydrodynamics, and kinetics processes of solidification vary here. To this end, a modification was analyzed with heating of the heat of the material that would assure an ~7 times reduction in the heat flux. At the initial time the domain with maximal value of the velocity is shifted to the lower third of the ingot (Fig. 1b), which is due to an analogous shifting of the maximal temperature gradient.

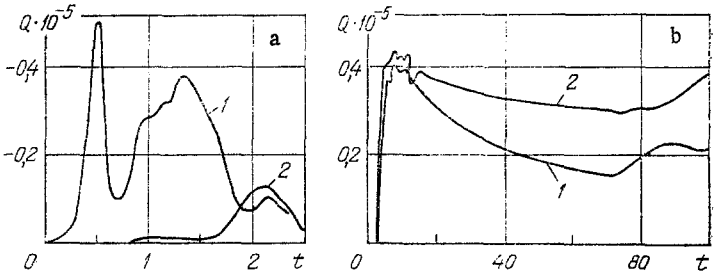

Fig. 3. Dependence of the heat flux Q (W) through the ingot head–body boundary on the time t (min) in the convection active phase period [a), convection damping and degeneration (b); 1) heating by chamotte; 2) heat-insulated inserts].

TABLE 1. Difference in the Thickness of the Solidified Metal Under Heating by Chamotte and by Heat Insulated Inserts

t, min	$\Delta t = r_{III} - e_{BJ}$, m	
	on the Oy axis	along Ox on the part under the head
5	$2{,}7\cdot10^{-5}$	$6{,}7\cdot10^{-4}$
10	$8{,}2\cdot10^{-4}$	$2{,}7\cdot10^{-3}$
20	$1{,}2\cdot10^{-3}$	$4{,}1\cdot10^{-3}$
30	$8{,}4\cdot10^{-5}$	$1{,}1\cdot10^{-3}$
40	$2{,}1\cdot10^{-4}$	$5{,}0\cdot10^{-3}$

As in the case of heating by chamotte, as solidification occurs the domain with maximal value of ψ is shifted to the parts under the head and at the head (Fig. 1d). The time to reach the greatest intensity of motion almost does not change but the intensity itself diminishes 1.5-2 times on the average (Fig. 2a) and the duration of the existence of convection increases.

Magnification of the heating reduces the rate of ingot congealing, especially its head part (Figs. 2b and c). The heat-transfer mode governs the kinetics of ingot shaping. Magnification of the heat insulation of the head part of the ingot diminishes the rate of horizontal solidification in its part under the head and has almost no effect on the vertical solidification rate (see Table 1).

A computation established that when materials with high heat insulation properties is used in the heater, a liquid crater (feeding channel) with high conicity and small depth as compared with the slightly heated ingot (Figs. 1e and f) is formed in the head and body of the ingot. This permits the assumption that a rise in the heat-insulating qualities of the heater will contribute to obtaining ingots with a smaller degree of damage by the primary shrinkage blisters, meaning, a higher quality.

NOTATION

$\theta = T/T_0$, $S = C/C_0$, $x = X/X_0$, $Fo = t\alpha/X_0^2$, $\vec{v} = \vec{V}/V_0$, ω, ψ, dimensionless temperature, true mean-volume concentration in the liquid phase, horizontal coordinate, time, mean-volume velocity, velocity vortex, and stream function; $Lu = \alpha/D$, $Pr = \nu_0/\alpha$, $Gr^* = g\beta T_0 X_0^3/\nu_0^2$, $W = L/c_2T_0$, Lewis, Prandtl, Grashof, and crystallization numbers, respectively; ξ, ξ_d, relative content of solid phase at an arbitrary macropoint and at the decanting boundary; T, T_k, ΔT_0, temperatures of a macropoint and of pure iron solidification, and of initial melt heating, °K; C, C_1, C_0, true mean-volume concentration in the liquid and solid phases, initial, wt. %; X, Y, X_0, H, horizontal and vertical coordinates, characteristic dimension of the domain (arithmetic mean of the upper and lower bases), domain height, m; t, time, sec; $\vec{V}$, V_x, V_y, $V_0 = \alpha/X_0$, true mean-volume velocity vector of the liquid phase, the horizontal and vertical velocity components, the characteristic velocity; α, ν_0, coefficient of thermal diffusivity and the kinetic coefficient of viscosity of the melt, m^2/sec; g, absolute value of the free-fall acceleration vector, m/sec^2; ρ, liquid phase density at T_0, kg/m^3; β, thermal coefficient of volume expansion, 1/K; Ω, mean volume value of the velocity vortex, 1/sec; L, latent heat

of crystallization, J/kg•K; λ_1, λ_2, solid and liquid phase heat conduction coefficients, W/m•K; k, equilibrium impurity distribution coefficient; α, slope of the liquidus line on the phase diagram, %K; q_0, characteristic heat flux, W/m^2; and c_1, c_2, solid and liquid phase specific heats, J/kg•K.

LITERATURE CITED

1. V. T. Borisov, V. V. Vinogradov, and I. L. Tyazhel'nikova, "State-of-the-art of the quasiequilibrium theory of a two-phase zone and its application to alloy solidification," Optimization of Thermophysical Casting Processes [in Russian], Inst. of Casting Processes, Academy of Sciences of the UkrSSR, Kiev (1977), pp. 39-59.
2. R. I. Nigmatulin, Principles of the Mechanics of Heterogeneous Media [in Russian], Nauka, Moscow (1978).
3. I. L. Vorob'ev, "Mathematical theory of casting crystallization," in: Problems of Automated Casting Production [in Russian], Trudy, MVTU, No. 330, Moscow (1980), pp. 31-51.
4. L. G. Loitsyanskii, Mechanics of Fluids and Gases [in Russian], Nauka, Moscow (1978).
5. Yu. A. Samoilovich and L. N. Yasnitskii, "Conjugate problem of heat transfer, hydrodynamics and solidification," Inzh.-Fiz. Zh., 41, No. 6, 1109-1118 (1981).
6. F. V. Nedopekin and S. S. Petrenko, "Mathematical model of binary alloy crystallization," Izv. Vyssh. Uchebn. Zaved., Chern. Metall., No. 7, 161 (1982).
7. V. A. Zhuravlev, S. P. Bakumenko, S. M. Sukhikh, et al., "On the theory of the formation of closed shrinkage cavities in alloy crystallization in large volumes," Izv. Akad. Nauk SSSR, Met., No. 1, 43-48 (1983).
8. Ya. A. Shneerov, V. F. Polyakov, and V. Ya. Minevich, "Temperature conditions of steel ingot heater operation," in: Metallurgy and Coke-Chemistry [in Russian], Tekhnika, Kiev (1975), pp. 81-84.
9. A. A. Samarskii, Theory of Difference Schemes [in Russian], Nauka, Moscow (1977).
10. F. F. Zavgorodnii, F. V. Nedopekin, and I. L. Povkh, "Hydrodynamics and heat transfer in a solidifying mode," Inzh.-Fiz. Zh., 33, No. 5, 922-930 (1977).
11. P. F. Zavgorodnii, F. V. Nedopekin, I. L. Povkh, and S. S. Petrenko, "Numerical investigation of the thermal convection of a solidifying melt in a turbulent regime," Dep. VINITI Oct. 16, 1980, No. 5304, Donetsk (1980).
12. J. W. Elder, "Laminar free convection in a vertical slot," J. Fluid Mech., 23, Pt. 1, 77-98 (1965).
13. A. G. Daikovskii, V. I. Polezhaev, and A. I. Fedoseev, "Investigation of the structure of the transition and turbulent convection regimes in a vertical layer," Izv. Akad. Nauk SSSR, Mekh. Zhidk. Gaza, No. 6, 66-75 (1978).
14. G. Z. Gershuni and E. M. Zhukovitskii, Convective Stability of Incompressible Fluids, Halsted Press (1976).
15. E. M. Kitaev, Solidification of Steel Ingots [in Russian], Metallurgiya, Moscow (1982).